The Role of the —OH Groups within Mn$_{12}$ Clusters in Electrocatalytic Water Oxidation

Naama Gluz,[a] George Christou,[b] and Galia Maayan*[a]

Abstract: The formidable reactivity of the oxygen-evolving center near photosystem II is largely based on its protein environment that stabilizes it during catalysis. Inspired by this concept, the water-soluble **Mn$_{12}$** clusters Mn$_{12}$O$_{12}$(O$_2$CC$_6$H$_3$(OH)$_2$)$_{16}$(H$_2$O)$_4$ (**3,5DHMn$_{12}$**) and Mn$_{12}$O$_{12}$(O$_2$CC$_6$H(OH)$_3$)$_{16}$(H$_2$O)$_4$ (**3,4,5THMn$_{12}$**) were developed as efficient electrocatalysts for water oxidation. In this work, the role of the —OH groups in the electrocatalytic process was explored by describing the structural and electrocatalytic properties of two new **Mn$_{12}$** clusters, **3,4DHMn$_{12}$** and **2,3DHMn$_{12}$**, having one —OH group in the *meta* position relative to the benzoate-Mn moiety, and one at the *para* or *ortho* position, respectively. The Mn centers in **3,4DHMn$_{12}$** were discovered to have lower oxidation potential compared with those in **2,3DHMn$_{12}$**, and thus, **3,4DHMn$_{12}$** can catalyze water oxidation with higher rate and TON than **2,3DHMn$_{12}$**. Hence, the role of the —OH groups in the electrocatalysis was established, being involved in electronic stabilization of the Mn centers or in proton shuttling.

Introduction

The oxygen-evolving complex (OEC) within photosystem II is a high oxidation state Mn$_4$CaO$_5$ cluster,[1] which catalyzes one of nature's most challenging reactions—the oxidation of water to protons and oxygen, while utilizing light as an energy source. As such, it has inspired chemists aiming to develop inexpensive, environmentally benign and efficient catalysts for water oxidation.[2,3] In the past years, various synthetic manganese complexes differing in their size and ligation have been extensively studied as structural and functional mimetic models of the OEC aiming to understand its structure–activity relationships towards the development of water oxidation catalysts.[2,4–12] The first examples of OEC mimics were small nuclearity complexes and clusters (Mn$_n$, $n = 1$–4) having structural elements similar to the OEC, and these enabled a reasonable starting point for investigating the structure-function relationship within the OEC.[4,8,11,12] However, their stability in water was limited and their catalytic water oxidation activity was based mostly on chemical oxidation.[2,10,11] In addition, turnover numbers (TONs) and oxygen evolution were usually very low, if at all demonstrated, probably due to the labile Mn^{II} and the irreversibility of the Mn^{III} as well as the instability of the Mn^{IV} formed during the catalytic cycle.[12,13]

A key to overcome these challenges is to mimic not only the structure of the OEC but also the protein environment about this catalyst, which maintains its stability during water oxidation turnover.[3,14–17] Specifically, the redox active tyrosine residue (containing an —OH group) and the adjacent histidine residue, can control the local pH about the active site via proton-shuttling pathways through the hydrogen-bonded amino acids network.[14,18] Mimicking nature's strategy by adjusting the ligation about the active site to have proton-accepting groups can be therefore useful in the design of artificial water oxidation catalysts.[17–21] These ligands can be either organic or inorganic;[22,23] the utilization of both types lead to the development of polynuclear high oxidation manganese clusters[24–26] as larger nuclearity mimics of the OEC.

The **Mn$_{12}$**-familiy—Mn$_{12}$O$_{12}$(O$_2$R)$_{16}$(H$_2$O)$_4$ (R = Me, Ph, etc.)[27]—represents an important structural mimic of the OEC, mimicking both the structure of the OEC as well as its protein environment.[28] The first synthesized member of this family is the one with R = Me (**Mn$_{12}$Ac**), which its structure was shown to be comprised of an inorganic Mn$_{12}$O$_{12}$ core (outer ring of 8 Mn^{III} ions oxo-bridged to inner cubene of Mn^{IV}$_4$O$_4$ (see Figure 1), bound to an organic periphery of 16 acetate ligands.[27] Under appropriate conditions, this organic periphery can be fully replaced by other carboxylates without affecting the core. Thus, **Mn$_{12}$Ac** serves as a precursor for many other members of this family. Modification of the organic ligands at the periphery allows a controlled tuning of the solubility and the redox potentials of the cluster.[27–31] Capitalizing on these properties, we recently reported on two unique **Mn$_{12}$** clusters: Mn$_{12}$O$_{12}$(O$_2$CC$_6$H$_3$(OH)$_2$)$_{16}$(H$_2$O)$_4$ (**Mn$_{12}$DH**),[28] in which the organic ligand is 3,5-dihydroxybenzoic acid (3,5-DHBA), and Mn$_{12}$O$_{12}$(O$_2$CC$_6$H$_2$(OH)$_3$)$_{16}$(H$_2$O)$_4$ (**Mn$_{12}$TH**),[31] in which the organic ligand is 3,4,5-trihydroxy benzoic acid (THBA). The di- and tri-

[a] N. Gluz, Dr. G. Maayan
Schulich Faculty of Chemistry
Technion—Israel Institute of Technology, Haifa (Israel)
E-mail: gm92@technion.ac.il

[b] Dr. G. Christou
Department of Chemistry, University of Florida, Gainesville, FL (USA)

Chemistry–A European Journal

Full Paper
doi.org/10.1002/chem.202100151

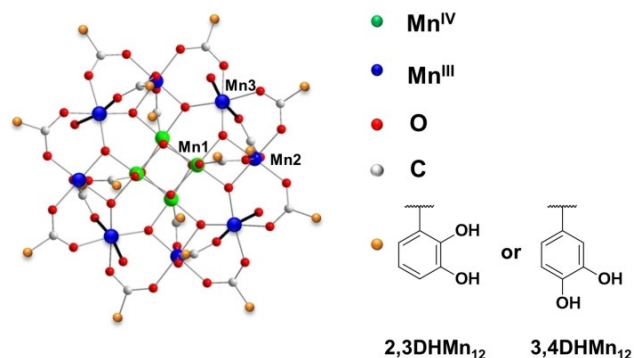**Chemistry Europe**
European Chemical
Societies Publishing

Figure 1. Designed structure of the water soluble **Mn$_{12}$** clusters, **2,3DHMn$_{12}$** and **3,4DHMn$_{12}$**, employing 2,3-DHBA and 3,4-DHBA as surrounding ligands.

Scheme 1. Possible ways for an –OH group to enhance water oxidation catalysis in water-soluble **Mn$_{12}$** clusters, depending on its position on the aromatic ring.

hydroxy-based ligands were incorporated to gain water-solubility and stability. The two clusters were explored as homogeneous water oxidation electrocatalysts and found to efficiently catalyze water oxidation at pH 6.[28,31] The results suggested that in addition to enabling the water solubility and stability of the cluster, the organic ligands might also play a role in the water oxidation activity, specifically the redox active hydroxyl groups that may enable proton shuttling similar to the –OH group of tyrosine in PSII.[28] Thus, it was shown that the additional –OH group in the *para* position of THBA, that was intentionally added to increase the proton-shuttling activity, led to a faster rate constant of **Mn$_{12}$TH** (630 folds faster) compared with the rate constant of **Mn$_{12}$DH**,[31] but its oxidation was irreversible. We therefore suggested that while the –OH groups in the *meta* position might enable proton shuttling leading to the high activity of **Mn$_{12}$DH**, the hydroxyl group in the *para* position do not have a role in proton shuttling, but rather serves to increase the electron density on the aromatic ring, which leads to a greater electronic stabilization of the high valent Mn ions, thus reducing the overpotential required for water oxidation.[31] This hypothesis, however, was not verified experimentally.

When located on an aromatic molecule, such as benzene, the –OH group is considered electron donating group by conjugation, and acts as an *ortho, para*-directing group; the *ortho* and *para* positions relative to the –OH are electron-rich while the *meta* position, is electronically not reactive.[32] Thus, when located at the *ortho* or *para* positions relative to a carboxylate group, for example, the –OH donates electron density from the lone pairs of the oxygen to the π system.[32] This analysis suggests that if at least one of the –OH groups located in the *meta* position on the benzoate rings within **Mn$_{12}$DH**, were instead located in the *ortho* or *para* positions relative to the carboxylate group, the electron density will be directed through the carboxylic moiety to the metal, stabilizing its high oxidation state (Scheme 1). In such clusters, the electron-rich aromatic ring would stabilize the metal better and its oxidation potential would be lowered, facilitating water oxidation, just like in the case of **Mn$_{12}$TH**. However, if the –OH groups in the *meta* positions play an important role in proton shuttling, which facilitates water oxidation also in the absence of electronic stabilization (Scheme 1), changing the position of one
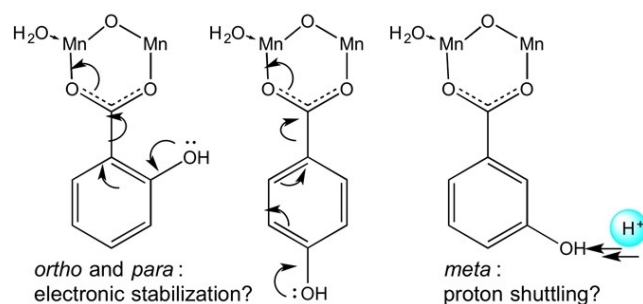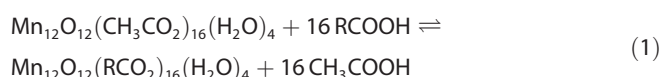
–OH group within **Mn$_{12}$DH** will not lead to clusters that are better water oxidation electrocatalysts than **Mn$_{12}$DH**. To further probe this hypothesis, herein we wish to explore the influence of the hydroxyl substituents, within the organic ligands surrounding the manganese core, on the catalytic activity of the cluster, by using ligands in which these substituents are located in different positions on the aromatic ring.
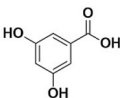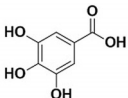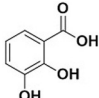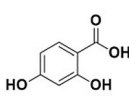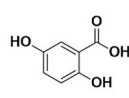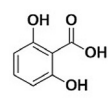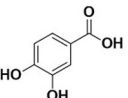
We would like to understand whether the position of the hydroxyl groups, in *ortho, meta* or *para* relative to the carboxylate group bound to the Mn^{III} ions, have a role in the electrocatalytic water oxidation activity, and if so, whether it involves electronic, structural, or other effects. To this aim, we wished to design new **Mn$_{12}$** clusters containing different isomers of 3,5-DHBA in which at least one of two hydroxyl groups is not in the *meta* position. The structure and properties of all the optional ligands are summarized in Table 1.

Mn$_{12}$ clusters are typically synthesized by the carboxylate substitution reaction [Eq. (1); R=C$_6$H$_3$(OH)$_2$], where the substitution equilibrium is driven to completion using an excess of a carboxylic acid ligand that its pK_a < 4.76 (the pK_a of acetic acid at 25 °C):[27]

$$Mn_{12}O_{12}(CH_3CO_2)_{16}(H_2O)_4 + 16\,RCOOH \rightleftharpoons$$
$$Mn_{12}O_{12}(RCO_2)_{16}(H_2O)_4 + 16\,CH_3COOH \tag{1}$$

In addition, we have previously found that in order to obtain a water-soluble **Mn$_{12}$** cluster, the carboxylate ligands should have high water solubility (> 10 g L^{-1}). Looking at the properties of the possible ligands depicted in Table 1, it is clear that the only two ligands that have both water solubility > 10 g L^{-1} and pK_a < 4.76 are 2,3-dihydroxybenzoic acid (2,3-DHBA) and 3,4-dihydroxybenzoic acid (3,4-DHBA), and these are the ligands we chose for this study. Using these ligands, we constructed two new **Mn$_{12}$** clusters, namely **3,4DHMn$_{12}$** containing 3,4-DHBA and **2,3DHMn$_{12}$** containing 2,3-DHBA, and examined their electrocatalytic activity. Constructing **Mn$_{12}$** clusters with these ligands allows a systematic study of water-soluble **Mn$_{12}$** clusters for understanding the structural, electronic, and mechanistic aspects of these clusters, for future development of stable and efficient Mn-based water oxidation catalysts.

Chemistry–A European Journal

Full Paper
doi.org/10.1002/chem.202100151

Chemistry Europe
European Chemical
Societies Publishing

Table 1. Water solubility and pK_a values (in water) of the di/tri-hydroxybenzoic acid ligands previously used for constructing water-soluble Mn_{12} clusters[28,31] (left), and of other dihydroxybenzoic acid isomers as optional ligands for this research (right).

Ligand	3,5-DHBA	THBA	2,3-DHBA	2,4-DHBA	2,5-DHBA	2,6-DHBA	3,4-DHBA
Water solubility at 25°C [g L^{-1}]	51	11.9	26.1	5.78	5.0	9.56	18.2
pK_a (COOH)	4.04	3.13	2.914	3.11	2.951	1.051	4.26

Results and Discussion

Synthesis and characterization of 2,3DHMn$_{12}$ and 3,4DHMn$_{12}$

As mentioned earlier, the readily available and inexpensive ligands, 2,3-DHBA and 3,4-DHBA, were chosen for their low pK_a values suitable for the carboxylate substitution reaction, their high water solubility essential for imparting solubility to the cluster, and for their desired electronic properties. The water soluble Mn_{12} clusters, $Mn_{12}O_{12}(O_2CC_6H_3(OH)O)_{16}(H_2O)_4$ (**2,3DHMn$_{12}$**) containing 2,3-DHBA and $Mn_{12}O_{12}(O_2CC_6H_3(OH)_2)_{16}(H_2O)_4$ (**3,4DHMn$_{12}$**) containing 3,4-DHBA, (Figure 1) were prepared in one step by treatment of **Mn$_{12}$Ac** with 40 equiv of 2,3-DHBA or 3,4-DHBA respectively in acetonitrile. The products were collected by filtration after one week, washed and dried, and found to be very soluble in water.

The solution of **3,4DHMn$_{12}$** in water had a typical brown color,[29–31] while the solution of **2,3DHMn$_{12}$** in water was dark green—a unique color for this type of clusters (Figure S1). This observation suggests that 2,3-DHBA might bind to the Mn-oxo core in a different binding mode than the typical carboxylate binding mode known for **Mn$_{12}$** clusters. The ligand 2,3-DHBA has several possible binding modes resulting from the structural proximity of the —OH substituent to the carboxylic acid; these include the typical bridging binding mode present in **Mn$_{12}$** clusters, which involves the carboxylic edge only,[27] and the salicylate binding mode that involves binding through the acid and the adjacent —OH substituent, as studied for various metals complexes employing such ligand[33–39] (Scheme 2). The
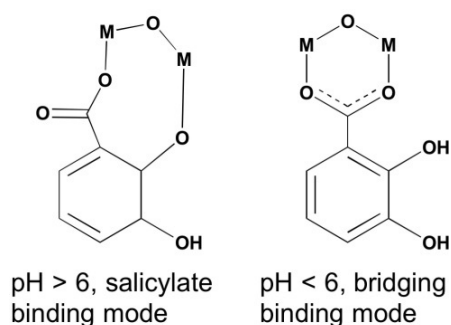
binding mode of 2,3-DHBA to metal centers should be pH controlled because it depends on the abstraction of the proton from the *ortho* —OH group. Thus, the salicylate binding mode will be preferred and stabilized in basic conditions at pH > 6 while the bridging binding mode should be stabilized in acidic conditions at pH < 6.

The clusters were structurally characterized by a collection of spectral and analytical methods, among them, UV/Vis and FTIR specifically, were expected to provide evidence for the salicylate type binding of the *ortho* —OH to the Mn ions.

Structural characterization of 3,4DHMn$_{12}$

The UV/Vis spectrum of **3,4DHMn$_{12}$** in un-buffered water (Figure S3A, red curve) showed two absorption bands at $\lambda_{max} = 250$ nm and $\lambda = 288$ nm, assigned to π–π^* and n–π^* transitions (comparable with the free ligand 3,4-DHBA: $\lambda = 252 + 289$ nm; Figure S3A, blue curve), and a broad shoulder near $\lambda = 334$ nm, assigned to ligand-to-metal charge transfer—an indication of cluster formation. The ATR-FTIR spectrum of a solid sample of **3,4DHMn$_{12}$** (Figure S4A) showed high similarity to the ATR-FTIR spectrum of **Mn$_{12}$DH** (Figure S4C) with some exceptions, originated from the nature of the 3,4-DHBA ligand (Table S1). These include the appearance of a new bend at 885 cm^{-1}, assigned to 1,3,4 tri-substituted benzene (based on a comparison between the spectra of **3,4DHMn$_{12}$** and its free ligand, 3,4-DHBA, Figure S8A) and a shift in ν (C—OH) band, relatively to **Mn$_{12}$DH**, which can be explained by the existence of hydrogen bonds between adjacent phenolic —OH groups in **3,4DHMn$_{12}$**. The multiple polar hydroxyl groups should give rise to many hydrogen-bonded interstitial water molecules in the solid state. This was confirmed by elemental analysis, presenting 17 hydrated water molecules and thus the molecular formula assigned to **3,4DHMn$_{12}$** is $[Mn_{12}O_{12}(O_2CC_6H_3(OH)_2)_{16}(H_2O)_4]\cdot17H_2O$. Thermogravimetric analysis (TGA) further supported this determination showing 8.67% experimental (8.23% calculated) weight loss, assigned to the release of hydrating water molecules between 100°C and 150°C (Figure S9A). ESI-MS analysis supported the cluster formation, and fragmentations of **3,4DHMn$_{12}$** were observed (calcd $m/2z = 1860.38$, found 1859.99, Figure S5). Overall, the structural characterization indicated the formation of the desired **3,4DHMn$_{12}$** cluster.

Scheme 2. The two possible binding modes of 2,3-dihydroxybenzoic acid (2,3-DHBA) in **Mn$_{12}$** clusters. The single Mn-benzoate unit is shown as a model that represents all the 16 units that exist in the **2,3DHMn$_{12}$** cluster.

Chemistry–A European Journal

Full Paper
doi.org/10.1002/chem.202100151

Chemistry Europe
European Chemical
Societies Publishing

Structural characterization of 2,3DHMn₁₂

The UV/Vis spectrum of **2,3DHMn₁₂** in un-buffered water (Figure S3 B, red curve) showed two absorption bands at $\lambda_{max} =$ 240 nm and $\lambda = 305$ nm, corresponding to $\pi–\pi^*$ and $n–\pi^*$ transitions (comparable with the free ligand 2,3-DHBA:[40] 238, 306 nm; Figure S3 B, blue curve), a broad band near $\lambda = 365$ nm assigned to ligand-to-metal charge transfer and an apparent d-d absorption band at 620 nm. Significantly, the later band supports the presence of a salicylate binding mode as it is only reported for Mn complexes in which the Mn ions are bound to the −OH group(s) of aromatic polyhydroxy ligands (typical d-d transitions are at the range between 550 and 750 nm).[39] In addition, UV/Vis spectroscopy measured in water and in different acetate buffers at pH values 4–7 (Figure S12) indicated that the salicylate binding mode, observed by the band at 620 nm, is pH dependent and preferred at pH ≥ 6. The ATR-FTIR spectrum of a solid sample of **2,3DHMn₁₂** (Figure S4 B) was also comparable to the ATR-FTIR spectrum of **Mn₁₂DH** with, again, some exceptions, originated from the nature of the 2,3DHBA ligand (Table S1). These include the appearance of a new bend at 788 cm⁻¹ corresponding to 1,2,3 tri-substituted benzene for **2,3DHMn₁₂** (based on comparison between the spectra of **2,3DHMn₁₂** and its free ligand, 2,3DHBA, Figure S8 B) and a shift in ν(C−OH) band relatively to **Mn₁₂DH**, which can be explained by the existence of strong hydrogen bonds between adjacent phenolic OHs and the carbonyl[40] in **2,3DHMn₁₂**. Importantly, a new peak at 1490 cm⁻¹, assigned to C−C ring stretching mode was observed, and this is a characteristic spectral feature of metal complexes employing the catechol-type ligands indicating the formation of a salicylate complex.[38,41] This peak supports the unique structure of **2,3DHMn₁₂** in which the *ortho* −OH group binds to the nearby Mn ion. Elemental analysis presented 12 hydrated water molecules for **2,3DHMn₁₂** and thermogravimetric analysis (TGA) further supported this determination showing 6.42 % experimental (6.05 % calculated) weight loss, assigned to the release of hydrating water molecules between 100 °C and 150 °C (Figure S9 B), thus suggesting that **2,3DHMn₁₂** has the formula [Mn₁₂O₁₂(O₂CC₆H₃(OH)O)₁₆(H₂O)₄]·12 H₂O.

ESI-MS analysis supported the clusters formation, and fragmentations of **2,3DHMn₁₂** were observed (calcd $m/4z = 892.88$, found 892.50, Figures S6 and S7). Even though the full mass could not be detected, the obtained masses were assigned to the cluster based on the high 4-fold symmetry of these clusters is presenting.[27] The structure of **2,3DHMn₁₂** was further supported by XPS analysis (Figures S10 and S11), showing two typical Mn−O peaks, with high similarity features to that of **Mn₁₂DH**, indicating that the oxidation states within **2,3DHMn₁₂** are the same as in **Mn₁₂DH**. The overall structural characterization indicates the formation of **2,3DHMn₁₂**.

Electrochemical characterization

Electrochemical characterization of the two ligands 3,4-DHBA and 2,3-DHBA and their corresponding clusters **3,4DHMn₁₂** and **2,3DHMn₁₂** was carried out by cyclic voltammetry (CV) and differential pulse voltammetry (DPV) measurements in acetate buffer at pH 6, the pH surrounding the OEC and the optimal pH for the electrocatalytic activity of **Mn₁₂DH** and **Mn₁₂TH**.[28,31] We note here that in these reaction conditions we do not expect the acetate ions from the solution to replace the benzoate ligands because the latter are more acidic than acetic acid and thus according to Equation (1) this displacement is not feasible. Moreover, a displacement of benzoate ligands by acetate ligands will lead to the formation of Mn₁₂ clusters that are not stable in aqueous solutions due to rapid hydrolysis, and a noticeable precipitate will form. As we do not observe such precipitation during the CV and CPE experiments we can rule out such displacement.

The CV of 3,4-DHBA (Figure 2 A) shows an oxidation wave at $E_p = 1.02$ V vs. NHE (onset point 0.55 V), attributed to the oxidation of the *para* −OH to the semiquinone. At the reverse side, a reduction wave appears at $E_p = 0.10$ V vs. NHE, attributed to the reduction of the semiquinone. The CV of **3,4DHMn₁₂** (Figure 2 A) exhibits three oxidation peaks: (i) oxidation of the *para* −OH group within the cluster at $E_p = 0.69$ V vs. NHE, (ii) two one-electron oxidation peaks, assigned to the oxidation of Mn3^(III/IV) and of Mn2^(III/IV) at $E_p = 1.13$ V and 1.58 V vs. NHE, respectively. In the reverse direction three cathodic peaks appear: Mn^IV to Mn^III reduction assigned to re-reduction of remaining oxidized cluster back to its resting state (Mn3 reduction) at $E_p = 0.85$ V, semiquinone reduction at $E_p = 0.10$ V and small peak of O₂ to superoxide reduction at $E_p = -0.60$ V vs. NHE.[42]

The CV of 2,3-DHBA at pH 6 acetate buffer (Figure 2 B) shows two oxidation waves at $E_p = 0.74$ V (onset point 0.45 V) and at $E_p = 1.62$ V vs. NHE, attributed to the oxidation of the *ortho* −OH group to form a semiquinone radical, followed by the oxidation of a *meta* −OH group to form a quinone, respectively.[31] No peaks on the reverse scan were observed, indicating that this process is irreversible. In the CV of **2,3DHMn₁₂** cluster (Figure 2 B), there are also three oxidation peaks: the oxidation of the *ortho* −OH group within the cluster at $E_p = 0.45$ V vs. NHE and the two Mn^III to Mn^IV oxidation peaks at $E_p = 1.03$ V (Mn3 oxidation) and 1.62 V (Mn2 oxidation) vs. NHE. In the back scan, two cathodic peaks appear: Mn^IV to Mn^III (Mn3) reduction at $E_p = 0.81$ V vs. NHE, and O₂ to superoxide reduction at −0.52 V vs. NHE. As the first oxidation wave is assigned to the oxidation of the unbound *ortho* −OH group and
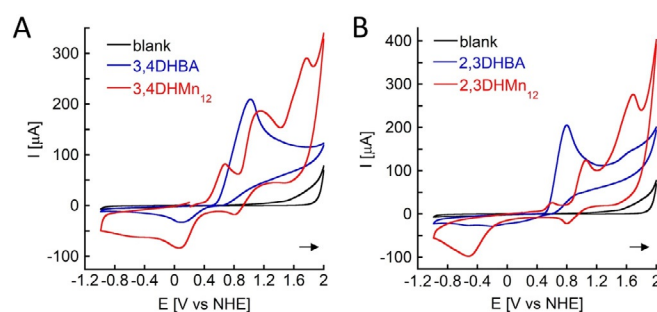

Figure 2. Cyclic voltammograms scanned at 100 mV s⁻¹ in the anodic direction of deoxygenated 0.1 M acetate buffer at pH 6 (black line) containing 8 mM of the free ligand 3,4DHBA (A, blue line), 2,3DHBA (B, blue line), 0.5 mM **3,4DHMn₁₂** (A, red line) or **2,3DHMn₁₂** (B, red line).

Chemistry–A European Journal

Full Paper
doi.org/10.1002/chem.202100151

Chemistry Europe
European Chemical
Societies Publishing

the soluble cluster kept its green color in these buffer conditions, we can suggest that at this pH (6), both binding modes, the bridging the salicylate, take place, with some of the **2,3DHMn₁₂** molecules and/or benzoate ligands in each cluster molecule binding in the bridging mode and some binding in the salicylate mode. CV scans of **2,3DHMn₁₂** taken in acetate buffer solution in the same reaction condition but at pH 5 or 4, show that the intensity of the oxidation peak near 0.45 V assigned to the oxidation of the *ortho* −OH group increases as the pH decreases (Figure S14). This is in line with our observation that the population of the cluster molecules with the ligand bound in the bridging mode increases at pH < 6, supporting our assumption that at pH 6, the two types of cluster molecules, in which the ligand is bound to the Mn center in the bridging mode or salicylate mode are present in the solution.

To further examine the electrochemical properties of the clusters, focusing on the Mn redox events, differential pulse voltammetry (DPV) was conducted for the two clusters in pH 6. The DPV results demonstrate well the influence of the different positions of the hydroxyl substituents in the ligands on the redox potential of the Mn ions within the cluster (Figure 3). Compared with **Mn₁₂DH**, in which the two $Mn^{III/IV}$ redox events occur near 1.01 V and 1.52 V vs. NHE, for Mn3 and Mn2 respectively (Figure 3C), for **3,4DHMn₁₂**, the two $Mn^{III/IV}$ events occur in lower potential, at 0.95 V and 1.5 V vs. NHE (Figure 3A). These results are in agreement with the ability of the *para*-hydroxyl substituent to donate electron density to the π system of the aromatic ring, which is directed through the carbonyl to the metal center (see Scheme 1). The increased electron density about the Mn ions leads to the stabilization of the $Mn^{III/IV}$ oxidation event and to a decrease its potential. **2,3DHMn₁₂** showed different behavior than expected: the first $Mn^{III/IV}$ redox event appears in a comparable potential to **Mn₁₂DH**, 1.02 V vs. NHE, but the second $Mn^{III/IV}$ event is shifted 200 mV to a higher potential and appears at 1.72 V vs. NHE, indicating thermodynamically less accessible ("destabilized") $Mn^{III/IV}$ oxidation event. (Figure 3B).

The destabilization of the $Mn^{III/IV}$ oxidation event may occur due to a more electron deficient environment about Mn2, that should be possible when the −OH substituent in the *ortho* position relative to the carboxylate is directly bound to the Mn ion, in the salicylate binding mode, which is the case for this cluster. In this binding mode, the oxygen of the hydroxyl substituent becomes an electron-withdrawing group leading to an electron deficient Mn2 center. As the oxo bridge between the Mn2 and Mn3 ions allows their electronic coupling and therefore charge de-localization,[22] once Mn2 is electron deficient, it can withdraw electron density from the nearby Mn3, making the oxidation of these Mn ions also less accessible.

Evaluation of the catalytic activity

The CV analysis of the two clusters already suggests catalytic water oxidation with an onset potential at ≈1.0 V vs. NHE and oxygen production as evident from the reduction peak of oxygen. In order to quantify the catalytic performances of the
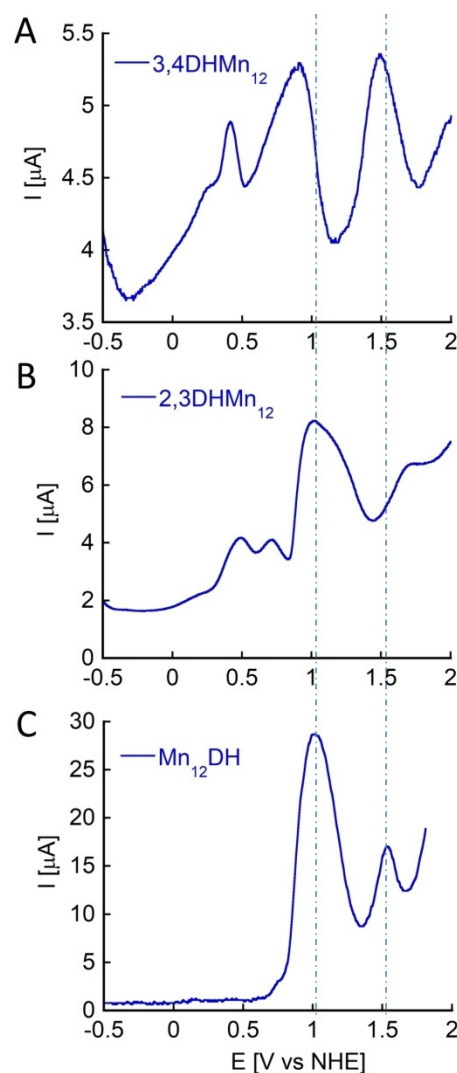

Figure 3. DPV scanned at 100 mV s⁻¹ in the anodic direction in deoxygenated 0.1 M acetate buffer at pH 6 containing 0.5 mM of **3,4DHMn₁₂** (A), **2,3DHMn₁₂** (B) and **Mn₁₂DH** (C). The vertical lines indicate the E_p of the two Mn^{III}/Mn^{IV} oxidation events of **Mn₁₂DH**.

clusters, controlled potential electrolysis (CPE) experiments were conducted for 5 hours at potential of 1.21 V vs. NHE, using solutions containing 2.5 μmol of each examined cluster in 5 mL 0.1 M pH 6 acetate buffer. These conditions were identical to those reported for **Mn₁₂DH**, aiming to compare between the electrocatalytic abilities of all three clusters and gain some understanding regarding the structure-function relationships. The evolution of molecular oxygen and the accumulated charge were monitored during the CPE reaction.

When **3,4DHMn₁₂** was used as a catalyst, 26.47 μmols of evolved O₂ were obtained and the total accumulated charge during this process was 19.75 C (Figure 4A, B, blue line), but only 16.52 μmols O₂ and 17.30 C were obtained when **2,3DHMn₁₂** was used as an electrocatalyst (Figure 4A, B, red line). The contribution of the blank, pH 6 acetate buffer (1.14 μmol O₂, and 2.19 C; Figure 4, black lines), was then subtracted and the turnover number (TON) and net Faradic efficiency (FE), calculated in 5 h, were 10.13 and 50.55%, respec-
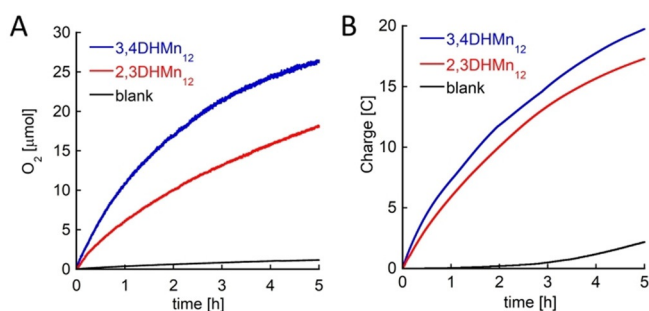
Chemistry–A European Journal

Full Paper
doi.org/10.1002/chem.202100151

Chemistry Europe
European Chemical
Societies Publishing

Figure 4. Evolution of O_2 during CPE, measured by a fluorescence-probe oxygen-meter in the headspace of the solution (A) and the CPE data showing charge passed versus time (B), for solutions containing 2.5 μmol **3,4DHMn$_{12}$** (blue lines) and 2.5 μmol **2,3DHMn$_{12}$** (red lines) in 5 mL 0.1 м pH 6 acetate buffer and for the buffer only (black lines), using a porous carbon working electrode at 1.21 V vs. NHE.

Figure 5. UV/Vis spectra (A) and ATR-FTIR spectra (B) of solution samples of **2,3DHMn$_{12}$**, which were collected during a 5 h CPE experiment at 1.21 V in acetate buffer at pH 6 (inset in A). The first sample to be collected (1) is marked in black, second (2): blue, third (3): red, fourth (4): green and fifth (5): orange.

tively, with **3,4DHMn$_{12}$** as an electrocatalyst, but only 6.60 and 42.89%, respectively with **2,3DHMn$_{12}$** as an electrocatalyst.

In order to verify that the water oxidation activity was due to the clusters and not the ligands, the ligands were tested in control experiments under the same conditions. CPE experiments for 8 mм 3,4-DHBA or 2,3-DHBA, yielded only a small amount of oxygen (about 6 μmol) for each ligand (Figure S15 A), but rather large amount of accumulated charge (about 14 C, Figure S15 B), indicating that ligand is undergoing oxidation but do not produce oxygen.

An interesting phenomenon, which was observed during the CPE reaction with **2,3DHMn$_{12}$** as a catalyst, is a color change of the solution, starting from dark green and ending with a dark brown colored solution. In addition, the pH during the CPE reaction decreased from 6 to 4.12. Knowing that the green color indicates the presence of cluster molecules in which the ligand binds to the Mn-oxo core in the salicylate mode rather than in the bridging mode and that the brown color and low pH signifies the absence of such molecules, we suggest that there is a structural change from the salicylate to the bridging binding mode during the CPE reaction. Such change is possible due to the flexibility of the carboxylic binding, and the presence of the adjacent —OH group. To probe this point and in order to understand the changes that **2,3DHMn$_{12}$** undergoes during the CPE reaction at pH 6, five samples of the solution containing the cluster were collected throughout a 5 h CPE experiment at 1.21 V and these samples were examined by UV/Vis and FTIR (Figure 5).

The UV/Vis spectra of the first three samples, showed a significant change in the LMCT band, described as a blue shift from 400 nm to 365 nm, a minor change in the 310 nm and 240 nm peaks, and a decrease of 620 nm band. These changes, assigned to the structural change of **2,3DHMn$_{12}$** from cluster molecules in which 2,3DHBA are bound to the Mn-oxo core in the salicylate binding mode to cluster molecules in which 2,3DHBA are bound in the bridging binding mode, result from the decrease in pH that occurs during the reaction (Figure 5 A). The most significant structural change takes place when the color of the solution changed from green (sample 3) to brown (sample 4), and this was reflected in the UV/Vis spectrum
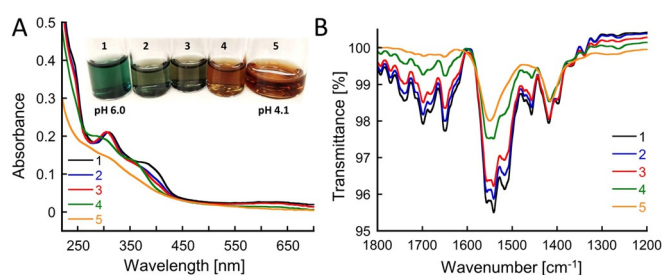
showing an increase of the 365 nm band together with full quenching of the 410 nm band, decrease in intensity and shifting of the 310 nm band and quenching of the 240 nm band. These changes indicate the full conversion of **2,3DHMn$_{12}$** in which 2,3DHBA are bound in the salicylate binding mode to cluster molecules in which 2,3DHBA are bound in the bridging binding mode. The decrease in the intensity of all the bands also suggests the oxidation of the —OH group(s).

This was further supported by CV experiments performed to each of the solutions 1–5, showing that the peak at 0.45 V, assigned to the oxidation of the *ortho* —OH group in the bridging mode changes during the electrolysis (Figure S16). In the beginning of the reaction, when the pH is 6, the current intensity of this peak is small, indicating that in most of the cluster molecules and/or that in most of the benzoate ligands in each cluster molecule the *ortho* —OH group binds in the salicylate mode. As the reaction proceed and the pH drops (samples 2 and 3), the intensity of this peak should increase due to the structural change of **2,3DHMn$_{12}$** and so there are more and more molecules and/or benzoate ligands in each cluster molecule in which the *ortho* —OH group binds in the bridging binding mode (as in Figure S14). However, due to the applied potential of the CPE, this —OH group is oxidized and thus the intensity of this peak decreases. As the reaction continues, this —OH group completely diminished (samples 4, 5) due to its full oxidation at the applied reaction potential.

The different functional groups, that is, the carboxylic and the phenolic —OH groups in **2,3DHMn$_{12}$** are distinguishable in the IR spectrum. ATR-FTIR was used to examine the samples of **2,3DHMn$_{12}$** collected during CPE (Figure 5 B), in order to determine spectroscopically whether the coordination mode of the ligand to the inorganic core is salicylate or bridging carboxylate. Changes in binding are usually observed by the appearance and/or disappearance of peaks, as well as peaks shift. The peaks pattern in the region of 1200–1300 cm^{-1} and 1600–1800 cm^{-1} is preserved and the main decrease in intensity is related to the structural change of **2,3DHMn$_{12}$** due to the pH drop. The change from salicylate coordination, involving carboxylic oxygen as well as the phenolic group, to the bridging carboxylate mode involving the two carboxylic oxygen atoms is evident in FTIR by several features:[41] (i) A downshift of the phenolic OH band at 1370 cm^{-1} to lower frequencies, creating

Chemistry–A European Journal

Full Paper
doi.org/10.1002/chem.202100151

Chemistry Europe
European Chemical
Societies Publishing

a broad shoulder at 1350 cm^{-1}, indicates the involvement of this functional group in the coordination, while the second phenolic band at 1336 cm^{-1} is unchanged. (ii) Disappearing of the band at 1399 cm^{-1}, assigned to symmetric (COO$^-$) stretching vibration. (iii) Disappearing of the bands at 1455 cm^{-1} and 1474 cm^{-1}, assigned to C–C ring stretching vibrations of the salicylate coordination -main evidence. (iv) Disappearing of the band at 1525 cm^{-1} assigned to C$_{aryl}$-H stretching vibrations. (v) The doublet at 1558 cm^{-1} and 1541 cm^{-1}, assigned to asymmetric (COO$^-$) stretching vibrations, is merged to a singlet band at 1548 cm^{-1}.

Overall, the information gathered from the structural analyses of **2,3DHMn$_{12}$** samples collected during CPE, demonstrates the structural change of **2,3DHMn$_{12}$** during the electrochemical water oxidation process.[43]

The role of the –OH groups on the electrocatalytic activity of polyhydroxy-Mn$_{12}$ clusters

The electronic and structural properties of **3,4DHMn$_{12}$** and **2,3DHMn$_{12}$** had a direct impact on their electrocatalytic properties as evident from the results of the CPE experiments conducted in the presence of each cluster at pH 6. These experiments showed that **3,4DHMn$_{12}$** is a better electrocatalyst for water oxidation than **2,3DHMn$_{12}$** and this is in correlation with the lower potential required for the oxidation of Mn2 and Mn3 ions. The cluster **3,4DHMn$_{12}$**, however, is a less efficient water oxidation electrocatalyst than **Mn$_{12}$DH**; this is surprising because the oxidation potentials of Mn2 and Mn3 in **3,4DHMn$_{12}$** are lower also from the oxidation potentials of the corresponding Mn ion in **Mn$_{12}$DH**. This results suggest that the –OH groups at the *meta* position of the benzoate ligands, not only have a role in the water oxidation process, but also that the contribution of one *meta* –OH group is larger than the contribution of a *para* –OH group. We have showed that the contribution of the *para* –OH groups to the reaction is based on the electronic stabilization of the Mn2 and Mn3 ions, resulting in favorable thermodynamics for carrying out water oxidation. It is also known that the –OH groups in the *meta* positions do not have such electronic stabilization effect.[44] Interestingly,

this apparent disadvantage allows protonation/de-protonation of the *meta* –OH groups and this should enable proton release, which is thought to be concurrent with the electron transfer process in the oxidative cycle of the OEC (PCET).[12] The –OH groups in the *meta* position can therefore serve as proton relies, which thus facilitate water oxidation to greater extent than the –OH group in the *para* position. Overall, we demonstrated that the organic shell of (poly)hydroxybenzoic acid-based **Mn$_{12}$** clusters, which can be considered as the second coordination sphere of the catalytic Mn-oxo core and was designed to solubilize and stabilize these in water, serves as an non-innocent ligand environment by playing a key role in the water oxidation process. We showed that within these **Mn$_{12}$** clusters, the hydroxyl substituents can either contribute or hamper electrocatalytic water oxidation, depending on their location on the aromatic ring: when located in the *para*- position to the benzoate-Mn moiety, the electron-donating –OH group helps stabilizing the high oxidation state Mn ions, enabling more favorable thermodynamics for carrying out water oxidation. When located in the *meta* position, the –OH groups may serve as proton relies and might be able to facilitate PCET processes and/or help removing protons generated in the water oxidation process, thus accelerating the catalytic process. When located in the *ortho* position, however, the –OH group can coordinate to the Mn-oxo core and this structural effect hampers water oxidation via destabilization of the Mn2 and Mn3 ions (Figure 6). From a comparison between the catalytic performances and the electrochemical properties of **2,3DHMn$_{12}$**, **3,4DHMn$_{12}$** and **Mn$_{12}$DH**, we can conclude that the contribution of proton relay to the catalytic process is greater than the contribution of the electronic effect.[5] This can explain the unusual activity of **Mn$_{12}$TH**, which its organic shell comprises of benzoate ligands with three –OH groups, all in positions that facilitate the water oxidation process (two in *meta* and one in *para*). This can also explain why the catalytic activity of **Mn$_{12}$DH**, having two –OH groups in the *meta* positions, is higher than the catalytic activity of **3,4DHMn$_{12}$** that has one –OH group in the *meta* position and one –OH group at the *para* position of the benzoate ligand. It is also clear now why the activity of **3,4DHMn$_{12}$** is higher than this of **2,3DHMn$_{12}$**,

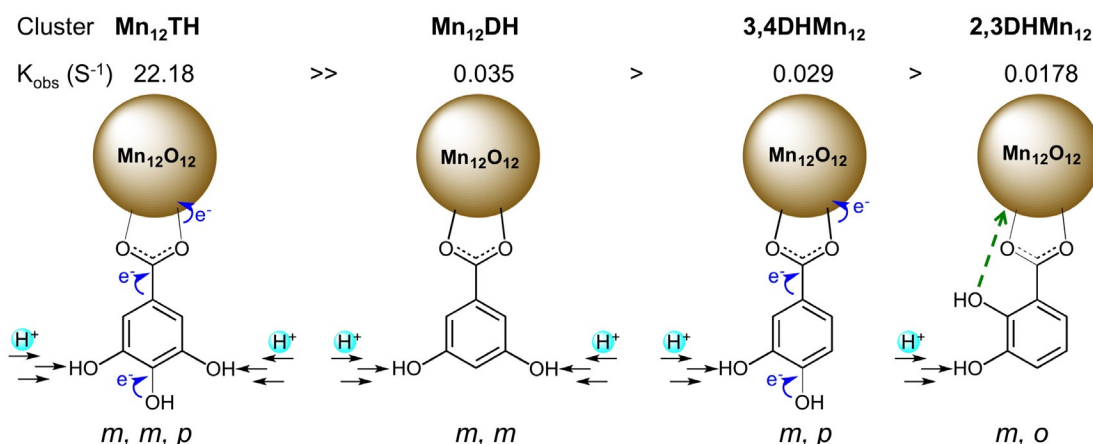| Cluster	**Mn$_{12}$TH**		**Mn$_{12}$DH**		**3,4DHMn$_{12}$**		**2,3DHMn$_{12}$**
K$_{obs}$ (S^{-1})	22.18	>>	0.035	>	0.029	>	0.0178

Figure 6. An illustration presenting the suggested contributions of hydroxyl moieties to water oxidation catalysis in several water-soluble **Mn$_{12}$** clusters.

Chemistry–A European Journal

Full Paper
doi.org/10.1002/chem.202100151

Chemistry
Europe
European Chemical
Societies Publishing

with only one —OH group in a contributing position (*meta*) but one —OH group in a destabilizing *ortho* position (Figure 6).

Homogeneity and kinetics of the two catalysts

In order to demonstrate that the clusters do not deposit on the electrode during the reaction, and serve as molecular soluble electrocatalysts, we conducted the following experiment: a CV of the blank, acetate buffer at pH 6, was scanned, then 0.5 mm of each cluster was added and 25 continuous CVs were recorded (Figure S18); the working electrode was then rinsed with water without polishing, placed in a fresh buffer and an additional CV was taken. A comparison between the two scans of the blank solutions taken with each cluster, suggests no deposition of the catalysts on the electrode surface (Figure S17). In order to further verify that the catalytic process is homogeneous, cyclic voltammograms in acetate buffer at pH 6 were recorded at different scan rates, in the range of 40–200 mV s^{-1} (Figure S19). The peak currents (i_p) of the two Mn oxidation events were plotted against the square root of the scan rate (Figure S20), and a linear fit was obtained for both Mn-oxidation events of the two clusters, confirming that the oxidation currents are diffusion controlled and the catalytic process in both cases is homogeneous. Furthermore, plotting the logarithm of the peak current, $\log(i_p)$, versus logarithm of the scan rate, $\log \nu$, for the two clusters (Figure S21) resulted in a straight line with a slope of 0.39 and 0.47 for **3,4DHMn$_{12}$** and **2,3DHMn$_{12}$** respectively for Mn3 oxidation event. These values are very close to the theoretical value of 0.5 that signifies an ideal reaction of a diffusion controlled electrode process.[45] For Mn2 oxidation event, slopes of about 0.69 and 0.73 were obtained for **3,4DHMn$_{12}$** and **2,3DHMn$_{12}$** respectively (Figure S21), suggesting a joint diffusion and adsorption control.[45] This can be assigned to the oxidation of both Mn2, which is diffusion controlled, and water oxidation, which involves the adsorption of water on the electrode surface. As both Mn3 and Mn2 oxidation events are homogeneous, we conclude that the overall oxidation process is also homogeneous throughout the catalytic cycle.

The CV data collected in different scan rates can also be used for obtaining k_{obs}, the apparent rate constant for the reaction. Foot-of-the-wave analysis (FOWA)[46] was performed, were we plotted i_{cat}/i_p vs. $1/(1 + \exp[(F/RT)(E_{cat}-E)])$ at each scan rate, and the value of k_{obs} was extracted from the slope of each plot. The catalysts **3,4DHMn$_{12}$** and **2,3DHMn$_{12}$** yielded averaged k_{obs} of 0.029 s^{-1} and 0.0178 s^{-1} respectively (Figure S22, Table S2). These values are consistent with the catalytic performances observed in CPE, that is, the cluster with bigger k_{obs} exhibited faster oxygen production in CPE, as indicated by the initial slopes in Figure 4 A and B.

Stability of the two catalysts

The stability of the two catalysts was examined by CV and UV/Vis measurements before and after 5 hours CPE at 1.21 V vs. NHE. In the cyclic voltammetry of the two clusters in pH 6 acetate buffer before (Figure S23, blue lines) and after (Figure S23,

red lines) CPE, the peaks assigned to the ligand disappeared due to the irreversible ligand oxidation, and the peak currents of the two Mn oxidation events slightly decreased and shifted to higher potential, probably due to the drop in pH (see Figure S14). However, for **2,3DHMn$_{12}$** (Figure S23, right) a big shift in the oxidation potential of the second Mn oxidation event was observed after CPE, meaning its oxidation is becoming more difficult and it might be more sensitive to pH change, due to the plausible structural change.

UV/Vis spectra of the clusters before and after CPE were measured in acetate buffer solutions at pH 6. The UV/Vis spectra of solutions containing the clusters after CPE (Figure S24) showed only small decrease in the absorbance of the characteristic peaks assigned to the ligand for **3,4DHMn$_{12}$** (Figure S24, left), but for **2,3DHMn$_{12}$** both shifting and quenching of the characteristic peaks are evident, and this is in agreement with ligand oxidation together with the structural change of **2,3DHMn$_{12}$** that occurs when the pH of the solution drops to pH 4 at the end of the catalytic reaction.

Conclusions

In the present work two new water-soluble **Mn$_{12}$** clusters, **3,4DHMn$_{12}$** and **2,3DHMn$_{12}$**, were synthesized, characterized by various analytical, spectroscopic, and electrochemical methods, and explored as water oxidation electrocatalysts. The electronic, structural and electrocatalytic properties of these clusters were thoroughly investigated in order to understand whether the —OH substituents on the benzoate ligands play a role in the catalytic water oxidation process, and if so, what is this role. The —OH substituents on an aromatic ring are considered electron donating groups by conjugation, where the *ortho* and *para* positions to the —OH are electron-rich.[32] Indeed, we discovered that shifting the —OH group from the *meta* position relative to the metal-carboxylate bond (as in **Mn$_{12}$DH**) to the *para* position (as in **3,4DHMn$_{12}$**) results in an increased stabilization of the high oxidation Mn ions as indicated by the lower Mn oxidation potentials observed in both the CV and DPV of **3,4DHMn$_{12}$** at pH 6. In contrast, shifting the —OH group to the *ortho* position (as in **2,3DHMn$_{12}$**) resulted in an unexpected decrease in the stabilization of the high oxidation Mn ions, demonstrated by the higher oxidation potentials of both Mn2 and Mn3 ions compared with those obtained in the DPV and CV of **Mn$_{12}$DH** or **3,4DHMn$_{12}$**. This result was further explained by the unique structure of **2,3DHMn$_{12}$**, in which the *ortho* —OH groups participate in the metal binding, and therefore their electrons are not accessible for stabilization of the metal ions via conjugation. Based on these findings we could establish the role of the —OH groups in each position, namely the *para*-, *meta*- or *ortho*- relative to the benzoate-Mn moiety within the polyhydroxy-**Mn$_{12}$** clusters, in the corresponding electrocatalytic water oxidation process. The new insights gathered in this research may be generalized to other benzoate substitutions different from —OH (ones that can have either electronic effect or proton-shuttling effect) towards the design of new and improved water-soluble Mn-based catalysts for water oxidation.

Chemistry–A European Journal

Full Paper
doi.org/10.1002/chem.202100151

Chemistry Europe
European Chemical
Societies Publishing

Experimental Section

Materials

Manganese(II) acetate tetrahydrate was purchased from Acros organics. $KMnO_4$ was purchased from Fisher chemicals. 2,3-dihydroxybenzoic acid and 3,4-dihydroxybenzoic acid were purchased from Alfa Aesar. Water (HPLC grade) and acetonitrile (HPLC grade) were purchased from Sigma Aldrich. Acetic acid, THF and diethyl ether were purchased from Gadot chemicals (Israel). Reagents and solvents were used without further purification. **$Mn_{12}Ac$** $[Mn_{12}O_{12}(O_2CMe)_{16}(H_2O)_4]$ was synthesized in a one-step comproportionation reaction of Mn^{II} acetate and $KMnO_4$ in aqueous acetic acid, according to a previously reported procedure.[47]

Synthesis

Synthesis of 3,4DHMn$_{12}$ $[Mn_{12}O_{12}(O_2CC_6H_3(OH)_2)_{16}(H_2O)_4]$: To a stirred solution of **$Mn_{12}Ac$**·$2MeCO_2H$·$4H_2O$ (0.25 g, 0.12 mmol) in acetonitrile (40 mL) 3,4-dihydroxybenzoic acid (0.74 g, 4.83 mmol) was added as a solid. The solution was left stirring for one week. The resulting dark brown precipitate was collected by filtration, washed with acetonitrile (3×15mL mL), THF (2×15ml), and diethyl ether (2×15 mL), and dried under vacuum. Yield: 77% (0.33 g 0.09 mmol) based on the **$Mn_{12}Ac$** precursor. The solid was analyzed as $[Mn_{12}O_{12}(O_2CC_6H_3(OH)_2)_{16}(H_2O)_4]$·$17H_2O$. Elemental analysis calcd for $C_{112}H_{122}Mn_{12}O_{97}$ (Mw = 3679 g mol^{-1}): C: 36.56; H: 3.34%; found: C: 36.52; H: 3.377%. The structure was verified by ESI-MS analysis (Figure S5), showing the mass of one half of cluster with $([Mn_{12}O_{12}(COOC_6H_3(OH)_2)_{16}(H_2O)_4]$·$19H_2O+Li^+)/2$ at 1859.99 m/z (calculated 1860.38 m/z), and isotopic distribution of a fragmented structure of $([Mn_{12}O_{12}(COOC_6H_3(OH)_2)_8(H_2O)_4]$·$9H_2O+2Li^+)/2$ at 1123.82 (calculated 1123.72 m/z). UV/Vis (Figure S3 A): $\lambda = 250$ nm and 288 nm: ligand transition bands (π–π*/n–π*), $\lambda = 334$ nm: ligand-to-metal charge transfer (shoulder). FTIR (Figure S4 A): $\tilde{v} = $ 750–500 (several Mn—O); 885 (1,3,4-tri-substituted benzene vibrations); 1260 (C—OH stretching), 1377 (symmetric COO stretching), 1539 (anti-symmetric COO stretching); 3300 cm^{-1} (O—H stretching, hydrogen bonded).

Synthesis of 2,3DHMn$_{12}$ $[Mn_{12}O_{12}(O_2CC_6H_3(OH)O)_{16}(H_2O)_4]$: To a stirred solution of **$Mn_{12}Ac$**·$2MeCO_2H$·$4H_2O$ (0.25 g, 0.12 mmol) in acetonitrile (40 mL), 2,3-dihydroxybenzoic acid (0.74 g, 4.83 mmol) was added as a solid. After few hours, the color of the solution was changed from dark brown to reddish-brown and the solution was left stirring for one week. The resulting dark green precipitate was collected by filtration, washed with acetonitrile (3×30mL mL), THF (2×20ml), and diethyl ether (2×20 mL), and dried under vacuum. Yield: 40% (0.17 g, 0.048 mmol) based on the **$Mn_{12}Ac$** precursor. The solid was analyzed as $[Mn_{12}O_{12}(O_2CC_6H_3(OH)O)_{16}(H_2O)_4]$·$12H_2O$. Elemental analysis calcd for $C_{112}H_{96}Mn_{12}O_{92}$ (Mw = 3573 g mol^{-1}): C: 37.65%, H: 2.71%; Found: C: 37.646%; H: 2.825%. The structure was verified by ESI-MS analysis, showing the mass of a quarter cluster with $C_{28}H_{24}Mn_3O_{23}$ at 892.50 m/z (calculated 892.88 m/z) (Figure S6 a and b). The theoretical isotopic distribution of Mn match the observed, showing $C_{28}H_{23}Mn_3O_{23}+K^+$ at 930.48 m/z (calculated 930.84 m/z) and $C_{28}H_{24}Mn_3O_{23}+2K^+$ at 970.42 m/z (calculated 970.81 m/z). (Figure S7 a and b). UV/Vis (Figure S3 B): $\lambda = 240$ and 305 nm: ligand transition bands (π–π*/ n–π*), $\lambda = 365$ nm: ligand-to-metal charge transfer, $\lambda = 610$ nm: d-d transitions. FTIR (Figure S4 B): $\tilde{v} = $ 750–500 (several Mn—O); 788 (1,2,3-tri-substituted benzene vibrations); 1250 (C—OH stretching), 1388 (symmetric COO stretching), 1558 (anti-symmetric COO stretching); 1490 (C—C ring stretching mode); 3300 cm^{-1} (O—H stretching, hydrogen bonded).

Equipment

Structural characterization: Elemental C, H, N, O analyses were performed using a "Thermo-Scientific Flash 2000 elemental organic analyzer". FTIR spectra (400–4000 cm^{-1}) were recorded on an "Agilent Cary 630" FTIR spectrometer, equipped with a diamond attenuated total reflection (ATR) instrument, allowing direct measurement with no sample preparation. UV/Vis spectroscopy measurements (200–800 nm) were performed on an "Agilent Cary 60" spectrometer at 25 °C using a 1 cm path length quartz cell. ESI-MS analysis was performed on a maXis impact Bruker Q-top mass spectrometer under electrospray ionization (ESI), in a positive ionization mode. TGA was performed using "Labsys Evo STA" (simultaneous thermal analysis) TGA analyzer (SETARAM instrumentations). A 15 mg sample was put in an open ceramic crucible and heated from room temperature up to 500 °C in flowing oxygen atmosphere (heating rate 10 °C min^{-1}) and a 5 min isotherm at 500 °C. X-ray photoelectron spectroscopy (XPS) measurement was performed in the solid-state institute at the Technion, on a "Thermo-VG SCIENTIFIC SIGMA probe" XPS spectrometer.

Electrochemical characterization: Cyclic voltammetry (CV) and differential pulse voltammetry (DPV) were conducted at room temperature using 563 model "IVIUMSTAT.XRe" potentiostat/galvanostat. The measurements were conducted in a standard three-electrode cell assembly consisting of a glassy carbon electrode as the working electrode, Pt mesh as the counter (auxiliary) electrode, and a Ag/AgCl/3 M KCl reference electrode (+210 mV vs. NHE). CVs were typically recorded at scan rate of 100 mV s^{-1}; E step of 10 mV and 0.1 mAV^{-1} sensitivity, in 0.1 M acetate buffer pH 6 containing 0.5 mM of the clusters or 8 mM of the free ligand. DPVs were recorded at scan rate of 100 mV s^{-1}; E step of 10 mV, pulse time 10 ms and pulse amplitude 20 mV, in 0.1 M acetate buffer pH 6 containing 0.5 mM of the clusters. No IR compensation was employed. The potential was measured vs. the Ag/AgCl reference electrode and converted to vs. NHE by using $E(NHE) = E(Ag/AgCl) + 0.21$ V. Deoxygenation was accomplished by bubbling N_2 through the solutions for 5 min.

Electrocatalytic experiments: Controlled potential electrolysis (CPE) experiments were performed in a three compartment 'H-cell' separated by a medium-porosity sintered glass frit. Three-electrode assembly was used consisting of vitreous carbon-3000C Foam as the working electrode, Pt mesh as the counter (auxiliary) electrode, and a Ag/AgCl/3 M KCl reference electrode (+210 mV versus NHE). 2.5 μmol of catalyst was loaded to the anodic compartment, equipped with working and reference electrodes. Deoxygenation was accomplished by bubbling argon stream at atmospheric pressure was bubbled into the cell for 20 minutes prior to scanning. The electrolysis was performed at potential of 1.21 V vs. NHE. Direct oxygen measurements during the CPE were carried out using a "PreSens Microx 4" stand-alone optic fiber oxygen meter and "Fire sting GO_2" needle type oxygen sensor (PyroScience GmbH) at the headspace of the electrochemical cell. Oxygen values were recorded in μM and %O_2 units and were translated to micromols of O_2 using calibrations curves, considering the RTP values of 24.465 L mol^{-1} O_2 at 25 °C and 1 atm conditions.

The μM O_2 and % O_2 values were converted to μmols O_2 by using Equations (2) and (3):

$$\mu mol\ O_2 = \{(\mu M\ value - 14.263)/0.1902\}/24.456 \tag{2}$$

$$\mu mol\ O_2 = \{(\%O_2\ value - 0.1066)/0.01385\}/24.456 \tag{3}$$

Faraday efficiency was determined according to the total charge passed during the CPE and the total amount of generated oxygen

by taking into account that water oxidation is a four-electron-oxidation process [Eq. (4)].

$$FE\ (\%) = \frac{4 \times mol\ of\ O_2 \times 100\%}{mol\ electrons} \qquad (4)$$

in which mol electrons = charge (C)/96485 C mol^{-1}.

Acknowledgements

Conflict of interest

The authors declare no conflict of interest.

[1] M. Suga, F. Akita, K. Hirata, G. Ueno, H. Murakami, Y. Nakajima, T. Shimizu, K. Yamashita, M. Yamamoto, H. Ago, J.-R. Shen, *Nature* **2015**, *517*, 99–103.

[2] M. D. Kärkäs, B. Åkermark, *Dalton Trans.* **2016**, *45*, 14421–14461.

[3] M. M. Najafpour, I. Zaharieva, Z. Zand, S. Maedeh Hosseini, M. Kouzmanova, M. Hołyńska, I. Tranca, A. W. Larkum, J.-R. Shen, S. I. Allakhverdiev, *Coord. Chem. Rev.* **2020**, *409*, 213183.

[4] C. Zhang, C. Chen, H. Dong, J.-R. Shen, H. Dau, J. Zhao, *Science* **2015**, *348*, 690–693.

[5] W. A. A. Arafa, M. D. Kärkäs, B.-L. Lee, T. Åkermark, R.-Z. Liao, H.-M. Berends, J. Messinger, P. E. M. Siegbahna, B. Åkermark, *Phys. Chem. Chem. Phys.* **2014**, *16*, 11950–11964.

[6] E. A. Karlsson, B.-L. Lee, T. Åkermark, E. V. Johnston, M. D. Kärkäs, J. Sun, Ö. Hansson, J.-E. Bäckvall, Björn Åkermark, *Angew. Chem. Int. Ed.* **2011**, *50*, 11715–11718; *Angew. Chem.* **2011**, *123*, 11919–11922.

[7] R. Brimblecombe, A. Koo, G. C. Dismukes, G. F. Swiegers, L. Spiccia, *J. Am. Chem. Soc.* **2010**, *132*, 2892–2894.

[8] C. S. Mullins, V. L. Pecoraro, *Coord. Chem. Rev.* **2008**, *252*, 416–443.

[9] R. Tagore, R. H. Crabtree, G. W. Brudvig, *Inorg. Chem.* **2008**, *47*, 1815–1823.

[10] A. K. Poulsen, A. Rompel, C. J. McKenzie, *Angew. Chem. Int. Ed.* **2005**, *44*, 6916–6920; *Angew. Chem.* **2005**, *117*, 7076–7080.

[11] J. Limburg, J. S. Vrettos, L. M. Liable-Sands, A. L. Rheingold, R. H. Crabtree, G. W. Brudvig, *Science* **1999**, *283*, 1524–1527.

[12] R. Manchanda, G. W. Brudvig, R. H. Crabtree, *Coord. Chem. Rev.* **1995**, *144*, 1–38.

[13] G. W. Brudvig, *Nat. Catal.* **2018**, *1*, 10–11.

[14] H. Dau, C. Limberg, T. Reier, M. Risch, S. Roggan, P. Strasser, *ChemCatChem* **2010**, *2*, 724–761.

[15] D. Narzi, D. Bovi, L. Guidoni, *Proc. Natl. Acad. Sci. USA* **2014**, *111*, 8723–8728.

[16] K. J. Young, B. J. Brennan, R. Tagore, G. W. Brudvig, *Acc. Chem. Res.* **2015**, *48*, 567–574.

[17] M. M. Najafpour, G. Renger, M. Hołyńska, A. N. Moghaddam, E.-M. Aro, R. Carpentier, H. Nishihara, J. J. Eaton-Rye, J.-R. Shen, S. I. Allakhverdiev, *Chem. Rev.* **2016**, *116*, 2886–2936.

[18] T. Zhang, C. Wang, S. Liu, J. L. Wang, W. Lin, *J. Am. Chem. Soc.* **2014**, *136*, 273–281.

[19] M. Zhang, Z. Chen, P. Kang, T. J. Meyer, *J. Am. Chem. Soc.* **2013**, *135*, 2048–2051.

[20] S. M. Barnett, K. I. Goldberg, J. M. Mayer, *Nat. Chem.* **2012**, *4*, 498–502.

[21] R. Matheu, P. Garrido-Barros, M. Gil-Sepulcre, M. Z. Ertem, X. Sala, C. Gimbert-Suriñach, A. Llobet, *Nat. Rev. Chem.* **2019**, *3*, 331–341.

[22] M. D. Kärkäs, O. Verho, E. V. Johnston, B. Åkermark, *Chem. Rev.* **2014**, *114*, 11863–12001.

[23] R. Al-Oweini, A. Sartorel, B. S. Bassil, M. Natali, S. Berardi, F. Scandola, U. Kortz, M. Bonchio, *Angew. Chem. Int. Ed.* **2014**, *53*, 11182–11185; *Angew. Chem.* **2014**, *126*, 11364–11367.

[24] J. Soriano-López, R. Elliott, A. C. Kathalikkattil, A. M. Ako, M. Mulahmetović, M. Venkatesan, W. Schmitt, *ACS Sustainable Chem. Eng.* **2020**, *8*, 13648–13659.

[25] C. Kozoni, E. Manolopoulou, M. Siczek, T. Lis, E. K. Brechin, C. J. Milios, *Dalton Trans.* **2010**, *39*, 7943–7950.

[26] "Structural Types in Oxide-Bridged Manganese Chemistry: Toward a Model of the Photosynthetic Water Oxidation Center": G. Christou, J. B. Vincent, *Metal Clusters in Proteins, ACS Symposium Series No. 372*, American Chemical Society, **1988**, Chapter 12.

[27] R. Bagai, G. Christou, *Chem. Soc. Rev.* **2009**, *38*, 1011–1026.

[28] G. Maayan, N. Gluz, G. Christou, *Nat. Catal.* **2018**, *1*, 48–54.

[29] Y. Yan, J. S. Lee, D. A. Ruddy, *Inorg. Chem.* **2015**, *54*, 4550–4555.

[30] N. Gluz, G. Maayan, *J. Coord. Chem.* **2018**, *71*, 1971–1984.

[31] T. Ghosh, G. Maayan, *Angew. Chem. Int. Ed.* **2019**, *58*, 2785–2790; *Angew. Chem.* **2019**, *131*, 2811–2816.

[32] J. Clayden, N. Greeves, S. Warren, in *Organic Chemistry*, 2nd ed., Oxford University Press, Oxford, **2012**, Chapter 21, pp. 483–491.

[33] D. Hatzipanayioti, K. Kontotheodorou, *Spectrochim. Acta Part A* **2011**, *78*, 949–960.

[34] S. K. Sahoo, R. K. Bera, M. Baral, B. K. Kanungo, *Acta Chim. Slov.* **2008**, *55*, 243–247.

[35] N. Türkel, U. Özer, *Russ. J. Coord. Chem.* **2005**, *31*, 213–217.

[36] V. Aletras, A. Karaliota, M. Kamariotaki, D. Hatzipanayioti, N. Hadjiliadis, *Inorg. Chim. Acta* **2001**, *312*, 151–162.

[37] D. Hatzipanayioti, A. Karaliota, M. Kamariotaki, A. Veneris, P. Falaras, *Trans. Met. Chem.* **1998**, *23*, 407–416.

[38] M. Kamariotaki, A. Karaliota, D. Stabaki, T. Bakas, S. P. Perlepes, N. Hadjiliadis, *Trans. Met. Chem.* **1994**, *19*, 241–247.

[39] K. D. Magers, C. G. Smith, D. T. Sawyer, *Inorg. Chem.* **1978**, *17*, 515–523.

[40] D. Hatzipanayioti, G. Tzeferakos, P. Petropouleas, *Chem. Phys.* **2008**, *345*, 119–129.

[41] M. V. Biber, W. Stumm, *Environ. Sol. Technol.* **1994**, *28*, 763–768.

[42] Control CVs conducted at pH 6 acetate buffer indicated that cluster oxidation is prompting the electrocatalytic water oxidation to oxygen for the two clusters: when the CV scan started from the cathodic direction, the O$_2$/O$_2^-$ reduction peak at −0.6 V vs. NHE (for **3,4DHMn$_{12}$**) and at −0.5 V (for **2,3DHMn$_{12}$**) was absent in the first cycle, but appeared in the following cycles, indicating that it arises from the cluster oxidation process (Figure S13).

[43] The contribution of the electronic effect to catalysis in the carboxylate mode compared to the salicylate mode is not discussed here, because the catalysis is poor anyway in acidic medium, as can be seen in the CVs of **2,3DHMn$_{12}$** at different pH values (Figure S14), and even thought the hydroxyl is becoming free, its electronic contribution is very minor, compared to the poor catalysis.

[44] P. Zanello, *Inorganic electrochemistry: Theory, Practice and Application*, The Royal Society of Chemistry, London, **2003**, chapter 13, pp. 579–585.

[45] J. Wu, W. Wang, M. Wang, H. Liu, H. Pan, *Int. J. Electrochem. Sci.* **2016**, *11*, 5165–5179.

[46] C. Costentin, S. Drouet, M. Robert, J. M. Savéant, *J. Am. Chem. Soc.* **2012**, *134*, 11235–11242.

[47] T. Lis, *Acta Crystallogr. Sect. B* **1980**, *36*, 2042–2046.